Procedia Computer Science

Volume 80, 2016, Pages 1061–1070

ICCS 2016. The International Conference on Computational Science

Trawl-Door Shape Optimization by Space-Mapping-Corrected CFD Models and Kriging Surrogates

Ingi M. Jonsson[1], Leifur Leifsson[1,2], Slawomir Koziel[1], Yonatan A. Tesfahunegn[1], and Adrian Bekasiewicz[1]

[1] Reykjavik University, Reykjavik, Iceland
[2] Iowa State University, Ames, Iowa, U.S.A.
ingij@ru.is, leifur@iastate.edu, koziel@ru.is, yonatant@ru.is, bekasiewicz@ru.is

Abstract
Trawl-doors are a large part of the fluid flow resistance of trawlers fishing gear and has considerable effect on the fuel consumption. A key factor in reducing that consumption is by implementing computational models in the design process. This study presents a robust two dimensional computational fluid dynamics models that is able to capture the nonlinear flow past multi-element hydrofoils. Efficient optimization algorithms are applied to the design of trawl-doors using problem formulation that captures true characteristics of the design space where lift-to-drag ratio is maximized. Four design variables are used in the optimization process to control the fluid flow angle of attack, as well as position and orientation of a leading-edge slat. The optimization process involves both multi-point space mapping, and mixed modeling techniques that utilize space mapping to create a physics-based surrogate model. The results demonstrate that lift-to-drag maximization is more appropriate than lift-constraint drag minimization in this case and that local search using multi-point space mapping can yield satisfactory design at low computational cost. By using global search with mixed modeling a solution with higher quality is obtained, but at a higher computational cost than local search.

Keywords: Trawl-doors, computational fluid dynamics, surrogate-based optimization, space mapping, kriging interpolation.

1 Introduction

Optimization of trawl-door shapes is a key in minimizing the fuel consumption of fishing trawlers (Jonsson, 2012; Hermannsson, 2014). Due to the complex fluid flow past the trawl-doors, accurate computational fluid dynamics (CFD) models are required to resolve the figures of merit (the forces acting on the trawl-doors). High cost of the CFD simulations renders the optimization problem computationally challenging when using conventional techniques.

This paper presents an application of surrogate-based optimization techniques to hydrodynamic shape optimization of trawl-doors. The approach exploits construction of fast data-driven

Selection and peer-review under responsibility of the Scientific Programme Committee of ICCS 2016

doi:10.1016/j.procs.2016.05.409

surrogate models developed from space-mapping-corrected variable-fidelity CFD simulations. The resulting surrogate model provides an accurate representation of the design space at a relatively low cost since it is constructed using fast physics models. The surrogate is iteratively optimized and updated using the local optimum as an infill point. The algorithm is applied to lift-to-drag maximization and lift-constrained drag minimization of multi-element trawl-doors involving four design variables controlling the angle of attack and the trailing-edge slat position and orientation. The optimized shapes are obtained at a relatively low cost.

2 Problem Formulation

The objective of this work is to optimize the shape and configuration of trawl-doors, where they are treated as an independent system. The conventional trawl-doors are not considered since recent studies have revealed that airfoil-shaped trawl-doors, as proposed by Jonsson (2012) and Hermannsson (2014) are much more efficient than the conventional shape. Here we consider trawl-doors that are constructed from airfoil-shaped elements with multi-element configurations. Three sets of configurations are presented, main element with leading-edge slat, trailing edge flap or both as shown in Fig. 1.

In this study there are two different objective function formulations. On one hand, we minimize the drag coefficient for a constant lift coefficient as done in Leifsson et al. (2015), and on the other we maximize the lift-to-drag ratio. The first objective is written as: $min \;\; C_d(\mathbf{x}) \;\; s.t. \;\; C_l(\mathbf{x}) = const.$, where C_l is the lift coefficient, C_d is the drag coefficient, and $\mathbf{x}$ is the vector of design variables. The second objective is written as: $max \;\; C_l(\mathbf{x})/C_d(\mathbf{x})$.

In this work, the shape of each element and the free-stream velocity V_∞ is held constant through the optimization process. The inclination and position of the leading-edge flap and the trailing-edge slat, as well as angle of attack are designable parameters. Then the vector of design variables for multi element trawl-door with leading-edge slat and trailing-edge flap can be written as $\mathbf{x} = [\; x_{slat}/c \;\; y_{slat}/c \;\; \theta_{slat} \;\; x_{flap}/c \;\; y_{flap}/c \;\; \theta_{flap} \;\; \alpha \;]^T$, where x_{slat}/c is the slat leading-edge position on the x-axis, y_{slat}/c is the slat leading-edge position on the y-axis, θ_{slat} is the inclination of the slat relative to the x-axis, x_{flap}/c is the flap leading edge position on the x-axis, y_{flap}/c is the flap leading-edge position on the y-axis, θ_{flap} is the inclination of the flap relative to the x-axis, α is the angle of attack relative to the x-axis and c is the chord length of the main element. Throughout this study the shape of the elements are normalized, so that $c = 1$. All design variables are subjected to bounds, that is $\mathbf{l} \leq \mathbf{x} \leq \mathbf{u}$, where $\mathbf{u}$ is the upper bound of the design variable vector and $\mathbf{l}$ is the lower bound.

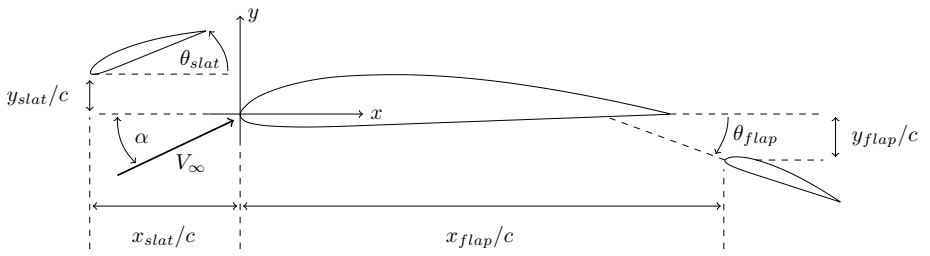

Figure 1: Two dimensional view of multi-element trawl-door constructed from airfoil shaped elements

3 Computational Fluid Dynamics Modeling

This section describes the computational fluid dynamics (CFD) modeling for trawl-door flow analysis in two-dimensions. In particular, the governing equations, computational grid, and flow solver are described. Furthermore, the section gives results of grid independence studies, and validation results.

3.1 Governing Equations

The flow is assumed to be steady, incompressible, viscous, and turbulent. Governing equations are the Reynolds-Averaged Navier-Stokes (RANS) equations with Menter's Shear-Stress Transport (SST) $k-\omega$ turbulence model. Refer to Tannehill and Anderson (1997) for further details on the governing equations and the SST $k-\omega$ turbulence model.

3.2 Flow Solver

The flow solver is coupled velocity-pressure-based formulation. The spatial discretization schemes are second order for all flow variables and the gradient is found by node based Green-Gauss method. Due to complex flow condition at high angles of attack a pseudo-transient option and high-order relaxation terms are used to obtain stable convergence. The solution controls were set with flow Courant number as 40, momentum and pressure relaxation factors were 0.10. The under relaxation factors for both turbulent kinetic energy and specific dissipation rate were set to 0.8, while higher order term relaxation factor for flow variables were set to 0.25.

3.3 Computational Grid

The goal was to have a grid with good quality and that could be generated both automatically and robustly according to updated geometries proposed by the optimizer. Unstructured triangular grid was chosen, it is generated more automatically and robustly when dealing with complex geometries than structured grids Mavriplis (1997). The far-field was configured with a box-topology, extending 100 main element chord-lengths c in all directions from the leading edge of the main element that was located in the center of the box. The far-field has to be located relatively far away from the trawl-door so that the flow generated by the boundary conditions is fully developed at the trawl-door for consistency of the flow solution. The triangular grid is clustered around the trawl-door geometry, and grows in size as it gets closer to the far-field where the maximum size is defined as $10c$. The initial size of the triangular grid, closest to the trawl-door is defined by the spacing between elements of the prismatic inflation layer that is extruded from all geometry surfaces. The role of the inflation layer is to capture characteristics of the boundary-layer and spacing between elements in stream-wise direction is determined by performing a grid convergence study. 10 prismatic layers were extruded from the geometry with exponential growth ratio of 1.2 and the initial layer height were set to $2.5e{-}5$ for the optimized geometries so that the non-dimensional wall distance $y^+ < 1$. An example grid is given in Fig. 2.

3.4 Convergence Study

Figure 3a shows a grid convergence study for a trawl-door with a NACA 2412 main element and a NACA 3210 leading edge slat placed at $x = -0.18$ $y = -0.08$. The length of the slat is 20% of the length of the main element and at an angle of 35°. The assembly is placed at an angle of

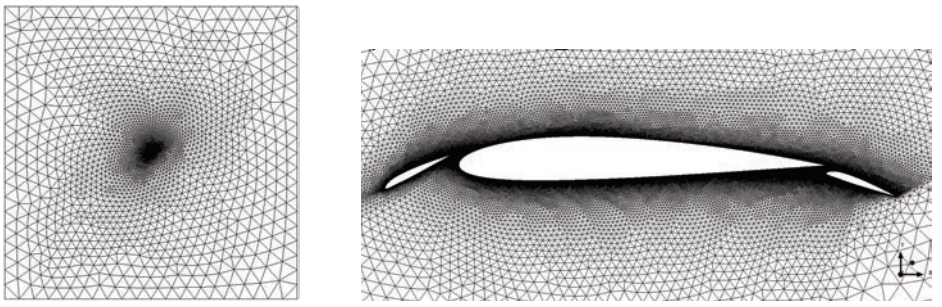

(a) Farfield (b) Close-up to the trawl-door

Figure 2: Example grid for multi-element trawl-door.

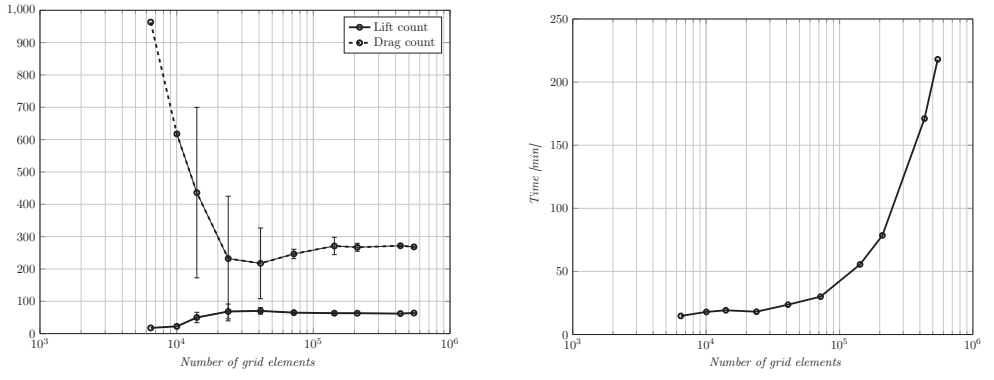

(a) (b)

Figure 3: Grid convergence study.

attack of 5° and the velocity were set at $2m/s$. It can be seen that the first three grid triplets consists of coarse and unreliable grids inheriting high uncertainties. The uncertainty reduces as the grids get finer and the solution more stabled, until it reaches a minimum at grid triplet seven where the solution is considered converged. For that reason grid number 9 with 4,800 elements distributed over the main element in stream-wise direction, resulting in total number of approximately 517,000 elements was chosen for the optimization process for this geometry. Figure 3b shows how the computational time increases as the total number of elements grow, resulting in a computational time of 170 minutes for the chosen grid.

4 Optimization Methodology

In this section, we describe the optimization methodology. In particular, we describe the general surrogate-based optimization algorithm, and surrogate construction for local and global searches. The local search is performed using multi-point output space mapping surrogates, and the global search with space-mapping-enhanced kriging surrogate models.

4.1 Surrogate-Based Optimization Algorithm

The optimization problem, discussed in Section 2, is cast as a nonlinear constrained minimization:

$$\mathbf{x}^* = \arg\min_{\mathbf{x}} H(\mathbf{f}(\mathbf{x})) \quad s.t. \quad \mathbf{g}(\mathbf{x})) \leq 0, \tag{1}$$

where $\mathbf{f}$ is the high-fidelity model response, H is the objective function, and $\mathbf{g}$ is an inequality constraint. The model response $\mathbf{f}(\mathbf{x}) = [C_{l,f} \quad C_{d,f}]^T$ where $C_{l,f}$ and $C_{d,f}$ are the lift and drag coefficients obtained by the high-fidelity model. For lift-to-drag maximization the objective function takes the form $H(\mathbf{f}(\mathbf{x})) = -C_{l,f}(\mathbf{x})/C_{d,f}(\mathbf{x})$, and for drag minimization $H(\mathbf{f}(\mathbf{x})) = C_{d,f}(\mathbf{x})$ with $\mathbf{g}(\mathbf{x}) = C_{l,t} - C_{l,f}(\mathbf{x})$ where $C_{l,t} = const.$.

In this work, we solve (1) by using the surrogate-based optimization (SBO) concept (Queipo et al., 2006; Forrester and Keane, 2009; Koziel, 2011; Koziel et al., 2013). The idea behind SBO is to replace direct optimization of an expensive computational model by an iterative process in which a sequence of designs approximating the solution to the original optimization problem is generated by means of optimizing a fast yet reasonably accurate representation of the high-fidelity model, referred to as a surrogate. In each iteration, the surrogate model is updated using the high-fidelity model evaluation at the most recent design (and, sometimes, some other suitably selected designs). Formally speaking, the surrogate-based optimization process can be written as (Koziel et al., 2013)

$$\mathbf{x}^{(i+1)} = \arg\min_{\mathbf{x}} H(\mathbf{s}^{(i)}(\mathbf{x})) \tag{2}$$

where $\mathbf{x}(i)$, $i = 0, 1, \ldots$, is a sequence of approximate solutions to the original problem (1), whereas $\mathbf{s}^{(i)}$ is the surrogate model at the ith iteration. $\mathbf{x}^{(0)}$ is the initial design.

The main prerequisite for the process (2) to be computationally efficient is the surrogate model $\mathbf{s}$ being significantly faster than the high-fidelity model $\mathbf{f}$. At the same time, the surrogate has to be sufficiently accurate (in terms of representing the high-fidelity model). In case of local search methods, reasonable accuracy is only requested in the vicinity of the current design $\mathbf{x}^{(i)}$. If both conditions are satisfied, the algorithm (2) is likely to quickly converge to the high-fidelity model optimum $\mathbf{x}^*$.

4.2 Local Search with Multi-Point Output Space Mapping Surrogates

A generic multi-point space mapping surrogate at iteration i in the SBO algorithm (2) (Koziel et al., 2006)

$$\mathbf{s}^{(i)}(\mathbf{x}) = \mathbf{s}(\mathbf{x}, \mathbf{p}^{(i)}), \tag{3}$$

where the parameters $\mathbf{p}$ are found by parameter extraction by solving a nonlinear minimization problem of the form

$$\mathbf{p}^{(i)} = \arg\min_{\mathbf{P}} \sum_{k=0}^{i} w_{i,k} \parallel \mathbf{f}(\mathbf{x}^{(k)}) - \mathbf{s}(\mathbf{x}^{(k)}, \mathbf{p}) \parallel^2, \tag{4}$$

where $w_{i,k}$ are weighting coefficients. The surrogate $\mathbf{s}$ can be constructed based on the model inputs $\mathbf{x}$, and $\mathbf{p}$ (input space mapping (Koziel et al., 2006)), or based the model outputs (output space mapping (Koziel and Leifsson, 2012)). In both cases, a low-fidelity model $\mathbf{c}$ is used in place of the high-fidelity model $\mathbf{f}$. $\mathbf{c}$ can be derived from simplified physics models,

coarse model discretization, or a combination of the two (see, e.g., (Leifsson and Koziel, 2015)). The minimization problem (4) aligns the surrogate model with the high-fidelity model using samples of both the high- and low-fidelity models gathered locally during the search process, i.e., minimized the difference of $\mathbf{f}$ and $\mathbf{s}$ in a least square sense using the samples at each design iteration $k = 0, 1, \ldots, i$.

For aero/hydrodynamic output responses from CFD models, Koziel and Leifsson (2012) suggested the following multi-point output space mapping surrogate form

$$\mathbf{s}^{(i)}(\mathbf{x}) = \mathbf{A}^{(i)} \circ \mathbf{c}(\mathbf{x}) + \mathbf{D}^{(i)} + \mathbf{q}^{(i)} = \left[a_l{}^{(i)} C_{l.c}(\mathbf{x}) + d_l{}^{(i)} + q_l{}^{(i)} \quad a_d{}^{(i)} C_{d.c}(\mathbf{x}) + d_d{}^{(i)} + q_d{}^{(i)} \right]^T, \tag{5}$$

where $\circ$ denotes component-wise multiplication, $\mathbf{c}$ is the low-fidelity model, and the response correction parameters $\mathbf{A}^{(i)}$ and $\mathbf{D}^{(i)}$ are obtained by solving

$$\left[\mathbf{A}^{(i)}, \mathbf{D}^{(i)} \right] = \arg \min_{[\mathbf{A},\mathbf{D}]} \sum_{k=0}^{i} \| \mathbf{f}(\mathbf{x}^{(k)}) - \mathbf{A} \circ \mathbf{c}(\mathbf{x}^{(k)}) + \mathbf{D} \|^2 . \tag{6}$$

The response scaling improves the matching for all points previously iterated. The additive response correction term $\mathbf{q}^{(i)}$ is defined as (Koziel and Leifsson, 2012)

$$\mathbf{q}^{(i)} = \mathbf{f}(\mathbf{x}^{(i)}) - \left[\mathbf{A}^{(i)} \circ \mathbf{c}(\mathbf{x}^{(i)}) + \mathbf{D}^{(i)} \right] \tag{7}$$

to make sure that there is perfect matching between the surrogate and the high-fidelity model at zero order consistency condition $\mathbf{x}^{(i)}, \mathbf{s}^{(i)}(\mathbf{x}^{(i)}) = \mathbf{f}(\mathbf{x}^{(i)})$.

The response correction parameters $\mathbf{A}^{(i)}$, $\mathbf{D}^{(i)}$ and the response scaling $\mathbf{q}^{(i)}$ can be calculated analytically (Koziel and Leifsson, 2012)

$$\begin{bmatrix} a_l{}^{(i)} \\ d_l{}^{(i)} \end{bmatrix} = (\mathbf{C}_l^T \mathbf{C}_l)^{-1} \mathbf{C}_l^T \mathbf{F}_l$$

$$\begin{bmatrix} a_d{}^{(i)} \\ d_d{}^{(i)} \end{bmatrix} = (\mathbf{C}_d^T \mathbf{C}_d)^{-1} \mathbf{C}_d^T \mathbf{F}_d \tag{8}$$

where

$$\mathbf{C}_l = \begin{bmatrix} C_{l.c}(\mathbf{x}^{(0)}) & C_{l.c}(\mathbf{x}^{(1)}) & \cdots & C_{l.c}(\mathbf{x}^{(i)}) \\ 1 & 1 & \cdots & 1 \end{bmatrix}^T$$

$$\mathbf{F}_l = \begin{bmatrix} C_{l.f}(\mathbf{x}^{(0)}) & C_{l.f}(\mathbf{x}^{(1)}) & \cdots & C_{l.f}(\mathbf{x}^{(i)}) \\ 1 & 1 & \cdots & 1 \end{bmatrix}^T \tag{9}$$

and

$$\mathbf{C}_d = \begin{bmatrix} C_{d.c}(\mathbf{x}^{(0)}) & C_{d.c}(\mathbf{x}^{(1)}) & \cdots & C_{d.c}(\mathbf{x}^{(i)}) \\ 1 & 1 & \cdots & 1 \end{bmatrix}^T$$

$$\mathbf{F}_d = \begin{bmatrix} C_{d.f}(\mathbf{x}^{(0)}) & C_{d.f}(\mathbf{x}^{(1)}) & \cdots & C_{d.f}(\mathbf{x}^{(i)}) \\ 1 & 1 & \cdots & 1 \end{bmatrix}^T \tag{10}$$

This is the least-square optimal solution to the linear regression problem $\mathbf{C}_l a_l^{(i)} + d_l^{(i)} = \mathbf{F}_l$ and $\mathbf{C}_d a_d^{(i)} + d_d^{(i)} = \mathbf{F}_d$, equivalent to (6).

4.3 Global Search with Space-Mapping-Corrected Kriging Surrogate Models

Koziel and Bandler (2007) suggested creating a surrogate by mixing data-driven methods (Queipo et al., 2006; Forrester and Keane, 2009) with physics-based surrogate models (Koziel et al., 2013; Leifsson et al., 2015). In this work, we follow the approach by (Koziel and Bandler, 2012) for modeling of microwave devices and construct a global surrogate model using kriging interpolation (Forrester and Keane, 2009) and enhance it with space mapping (Koziel and Leifsson, 2012). More specifically, the low-fidelity model $\mathbf{c}$ is used to construct the kriging model and the output space mapping technique is used correct it using a limited amount of high-fidelity model $\mathbf{f}$ samples.

Using (5), the output space mapping surrogate is then given by

$$\mathbf{s}^{(i)}(\mathbf{x}) = \mathbf{A}^{(i)} \quad \circ \quad \tilde{\mathbf{s}}(\mathbf{x}) + \mathbf{D}^{(i)} = \left[{a_l}^{(i)} C_{l.\tilde{s}}(\mathbf{x}) + {d_l}^{(i)} \quad {a_d}^{(i)} C_{d.\tilde{s}}(\mathbf{x}) + {d_d}^{(i)} \right]^T, \tag{11}$$

where $\tilde{\mathbf{s}} = [C_{l.\tilde{s}} \quad C_{d.\tilde{s}}]^T$ is the kriging surrogate model. The parameters $\mathbf{A}^{(i)}$ and $\mathbf{D}^{(i)}$ are still calculated using (8)-(10), but with $\tilde{\mathbf{s}}$ in place of $\mathbf{c}$.

Kriging is a Gaussian process based modeling method, which is compact and cheap to evaluate Journel and Huijbregts (1981); Simpson et al. (2001); Kleijnen (2009); Rasmussen and Williams (2005). In its basic formulation, kriging assumes that the function of interest is of the following form Journel and Huijbregts (1981); Simpson et al. (2001)

$$\mathbf{f}(\mathbf{x}) = \mathbf{g}(\mathbf{x})^T \boldsymbol{\beta} + Z(\mathbf{x}), \tag{12}$$

where $\mathbf{g}(\mathbf{x}) = [g_1(\mathbf{x}) \; g_2(\mathbf{x}) \; \dots g_K(\mathbf{x}) \;]^T$ are known (e.g., constant) functions, $\boldsymbol{\beta} = [\beta_1 \beta_2 \dots \beta_k]^T$ are the unknown model parameters (hyperparameters), and $Z(\mathbf{x})$ is a realization of a normally distributed Gaussian random process with zero mean and variance σ^2. The regression part $\mathbf{g}(\mathbf{x})^T \boldsymbol{\beta}$ is a trend function for $\mathbf{f}$, and $Z(\mathbf{x})$ takes into account localized variations. The covariance matrix of $Z(\mathbf{x})$ is given as

$$Cov\left[Z(\mathbf{x}^{(i)})(\mathbf{x}^{(j)}) \right] = \sigma^2 \mathbf{R} \left(\left[R(\mathbf{x}^{(i)}, \mathbf{x}^{(j)}) \right] \right), \tag{13}$$

where $\mathbf{R}$ is a $p \times p$ correlation matrix with $R_{ij} = R(\mathbf{x}^{(i)}, \mathbf{x}^{(j)})$. Here, $R(\mathbf{x}^{(i)}, \mathbf{x}^{(j)})$ is the correlation function between sampled data points $\mathbf{x}^{(i)}$ and $\mathbf{x}^{(j)}$. The most popular choice is the Gaussian correlation function

$$R(\mathbf{x}, \mathbf{y}) = exp\left[-\sum_{k=1}^{n} \theta_k \left| x_k - y_k \right| \right], \tag{14}$$

where θ_k are the unknown correlation parameters, and x_k and y_k are the kth components of the vectors x and y, respectively. The kriging predictor is defined as

$$\tilde{\mathbf{s}}(\mathbf{x}) = \mathbf{g}(\mathbf{x})^T \boldsymbol{\beta} + \mathbf{r}^T(\mathbf{x}) \mathbf{R}^{-1} (\mathbf{F} - \mathbf{G}\boldsymbol{\beta}), \tag{15}$$

where $\mathbf{r}(\mathbf{x}) = \left[R(\mathbf{x}, \mathbf{x}^{(1)}) \dots R(\mathbf{x}, \mathbf{x}^{(p)}) \right]^T$, $\mathbf{F} = \left[\mathbf{f}(\mathbf{x}^{(1)}) \quad \mathbf{f}(\mathbf{x}^{(2)}) \quad \dots \quad \mathbf{f}(\mathbf{x}^{(p)}) \right]^T$, and $\mathbf{G}$ is a $p \times K$ matrix with $G_{ij} = g_j(\mathbf{x}^{(i)})$. The vector of model parameters $\boldsymbol{\beta}$ can be computed as $\boldsymbol{\beta} =$

$(\mathbf{G}^T\mathbf{R}^{-1}\mathbf{G})^{-1}\mathbf{G}^T\mathbf{R}^{-1}\mathbf{f}$. Model fitting is accomplished by maximum likelihood for $\boldsymbol{\theta}_k$ Journel and Huijbregts (1981).

5 Numerical Example

This section presents the results of a numerical example illustrating the proposed approach applied to the design of a trawl-door shape with a main element and a leading-edge slat.

5.1 Description

The high-fidelity model has about 517,000 elements (grid 9). The flow solver convergence criteria were set to 5,000 iterations, or when residuals had dropped by six orders of magnitude. The low-fidelity model is the same as the high-fidelity one, but with a coarser mesh discretization and relaxed convergence criteria. The selected grid has about 15,000 elements (grid 4) and the model is considered converged after a fixed number of 500 flow solver iterations. The low fidelity model is on average around 78 times faster than the high-fidelity one.

The problem formulation is discussed in Section 2. We perform two local searches using multi-point output space mapping (described in Section 4.2), one for each objective function setup (as described in Section 4.1), and one global search (described in Section 4.2).

The flow speed is set to 2 m/s. The search space is defined as: $-0.35 \leq x_{flap}/c \leq -0.17$, $-0.08 \leq y_{flap}/c \leq 0.07$, $10 \leq \theta_{flap} \leq 40$ deg, $5.0 \leq \alpha \leq 35$ deg. The initial design is set as $x_{flap}/c = -0.2$, $y_{flap}/c = -0.08$, $\theta_{flap} = 25$ deg and $\alpha = 8$ deg.

5.2 Results

Table 1 summarizes the optimization results. When all the optimization results are examined, they all yield satisfactory results. In all of the cases, optimum results for design variable x_{slat}/c is within the range of $-0.200 \leq x_{slat}/c \leq -0.205$ and y_{slat}/c within $-0.0558 \leq x_{slat}/c \leq -0.0800$ whether the objective is to maximize C_l/C_d or minimize C_d. Even though the consistency is not as good between simulation results for design variables θ and α, the solutions are considered valid. The reason is that there are more than one equally good solutions for the problem at hand.

The highest lift-to-drag ratio of 82.1 is obtained by using global search. However, the difference between the two search methods is negligible considering the numerical noise present in the simulations. The case where the objective is to minimize C_d for given lift is not considered comparable in context of lift-to-drag values. Even though the nature of the problem requires the solution to be on top part of the lift-to-drag curve it is not constraint to the highest point.

If computational efficiency of the optimization runs is examined, the global search needs the longest computational time. The reason is a high number of low-fidelity evaluations, even though the low-fidelity model is computationally inexpensive compared to the high-fidelity one the high number of 900 evaluations take over 63 hours to compute. The advantages of this method are that the number of evaluations are directly related to the size of the search space (i.e., a smaller search space may translate to fewer evaluations). Another advantage is that only one high-fidelity evaluation is needed after the kriging surrogate has been constructed. Figure 4 shows the space-mapping-corrected kriging surface.

There is also much difference in computational time of the optimization process using multi-point SM. The case that minimizes C_d needs much higher number of both low- and high-fidelity evaluations. In that optimization run, the low-fidelity model is of lower quality than in the other

Table 1: Numerical results.

	Local Search I	**Local Search II**	**Global Search**
Objective	min C_d, $C_l \geq 1.2$	max C_l/C_d	max C_l/C_d
$\mathbf{x/c_{slat}}$	-0.200	-0.200	-0.205
$\mathbf{y/c_{slat}}$	-0.0630	-0.0800	-0.0558
$\boldsymbol{\theta}$ $[deg]$	24.1	29.3	25.5
$\boldsymbol{\alpha}$ $[deg]$	8.38	12.3	10.7
$\mathbf{C_l}$	1.20	1.67	1.48
$\mathbf{C_d}$	0.0150	0.0204	0.0180
$\mathbf{C_l/C_d}$	78.4	81.8	82.1
Evaluations HF/LF	14/400	4/83	1/900
Runtime gain ratio	≈ 78	≈ 18	-
Total runtime [hours]	≈ 55	≈ 19	≈ 67

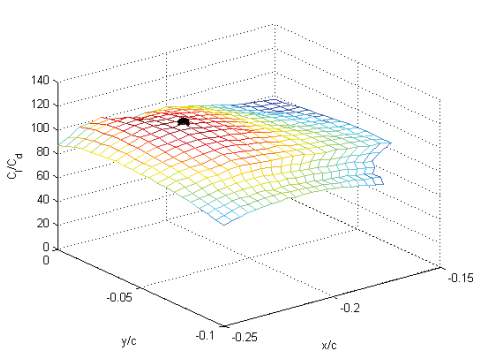

(a) The black dot represents the optimum solution

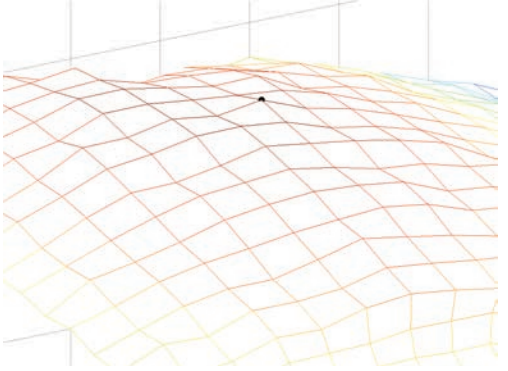

(b) Closer view

Figure 4: Slice parallel to the x_{slat}/c, y_{slat}/c surface of the kriging model at optimum location of $\theta = 20.5$ $deg.$ and $\alpha = 10.7$ $deg.$

cases, but instead the computational time for each low-fidelity evaluation is much lower. This difference is also affected by the objective value needed for the model to be converged.

6 Conclusion

A computationally efficient optimization methodology for the hydrodynamic design of multi-element trawl-door shapes using high-fidelity two-dimensional CFD models has been presented. Our approach exploits variable-fidelity models corrected using space mapping, and kriging interpolation surrogates. Numerical design studies of multi-element trawl-door shapes illustrate that satisfactory designs can be obtained at a low computational cost.

References

J. Forrester and A. Keane. Recent advances in surrogate-based optimization. *Progress in Aerospace Sciences*, 45:50–79, 2009.

E. Hermannsson. Hydrodynamic shape optimization of trawl doors with three-dimensional computational fluid dynamic models and local surrogates. Master's thesis, KTH Royal Institute of Technology, 2014.

E. Jonsson. Aerodynamic optimization by variable-resolution modeling and space mapping. Master's thesis, School of Science and Engineering, Reykjavik University, 2012.

A. Journel and C. Huijbregts. Neural network inverse modeling and applications to microwave filter design. *IEEE Transactions on Microwave Theory and Techniques*, 56:867–879, 1981.

J. Kleijnen. Kriging metamodeling in simulation: a review. *European Journal of Operational Research*, 192:707–716, 2009.

S. Koziel. Reliable design optimization of microwave structures using multipoint-response-correction space mapping and trust regions. *International Journal of RF and Microwave Computer-Aided Engineering*, 21:534–542, 2011.

S. Koziel and J. Bandler. Microwave device modeling using space-mapping and radial basis functions. *IEEE MTT-S Int. Microwave Symposium Digest*, 55:799–802, 2007.

S. Koziel and J. Bandler. Accurate modeling of microwave devices using kriging-corrected space mapping. *International Journal of Numerical Modelling*, 25:1–4, 2012.

S. Koziel and L. Leifsson. Knowledge-based airfoil shape optimization using space mapping. In *30th AIAA Applied Aerodynamics Conference*, 2012.

S. Koziel, J. Bandler, and K. Madsen. Theoretical justification of space-mapping-based modeling utilizing a data base and on-demand parameter extraction. *IEEE Trans. Microwave Theory Tech.*, 54:4316–4322, 2006.

S. Koziel, L. Leifsson, and S. Ogurtsov. *Surrogate-Based Modeling and Optimization. Applications in Engineering*. Springer, 2013.

L. Leifsson and S. Koziel. Variable-resolution shape optimization: low-fidelity model selection and scalability. *Int. J. of Mathematical Modelling and Numerical Optimisation*, 6:1–21, 2015.

L. Leifsson, E. Hermansson, and S. Koziel. Optimal shape design of multi-element trawl-doors using local surrogate models. *Journal of Computational Science*, 10:55–62, 2015.

D. Mavriplis. Unstructured grid techniques. *Fluid Mechanics*, 29:473–514, 1997.

N. Queipo, R. Haftka, W. Shyy, T. Goel, R. Vaidynathan, and P. Tucker. Surrogate-based analysis and optimization. *Progress in Aerospace Sciences*, 41:1 – 28, 2006.

C. Rasmussen and C. Williams. *Gaussian Processes for Machine Learning*. The MIT Press, 2005.

T. Simpson, T. Maurey, J. Korte, and F. Mistree. Kriging models for global approximation in simulation-based multidisciplinary design optimization. *AIAA Journal*, 39:2233–2241, 2001.

J. Tannehill and D. Anderson. *Computational Fluid Mechanics and Heat Transfer*. Taylor & Francis, 1997.